Using a neural network – Physics-based hybrid model to predict soil reaction fronts

Tao Wen [a,1,*], Chacha Chen [b,f,1], Guanjie Zheng [b,g], Joel Bandstra [c], Susan L. Brantley [d,e]

[a] *Department of Earth and Environmental Sciences, Syracuse University, Syracuse, NY, 13244, USA*
[b] *College of Information, Science and Technology, Pennsylvania State University, University Park, PA, 16802, USA*
[c] *Department of Mathematics, Engineering, and Computer Science, Saint Francis University, Loretto, PA, 15940, USA*
[d] *Earth and Environmental Systems Institute, Pennsylvania State University, University Park, PA, 16802, USA*
[e] *Department of Geosciences, Pennsylvania State University, University Park, PA, 16802, USA*
[f] *Now at Department of Computer Science, The University of Chicago, Chicago, IL, 60637, USA*
[g] *John Hopcroft Center for Computer Science, Shanghai Jiaotong University, Shanghai, 200240, China*

ARTICLE INFO

ABSTRACT

Analytical and numerical solutions have been proposed to model reaction fronts to study soil formation. With growing access to large geo-datasets and powerful computational capacity, data-driven models are becoming increasingly useful. We therefore explored the use of a neural network (NN) guided by a physics-based model (PBM) to simulate the depth profile of feldspar dissolution in soils. Specifically, we explored this hybrid neural network (HNN) to see if it could predict reaction fronts as a function of important variables known from domain knowledge: site climate characteristics (temperature T; precipitation P), geomorphic parameters (soil residence time t; erosion rate E), and parent material mineralogy (quartz content Q; albitic feldspar content of the feldspar A). We evaluated the mean square error (MSE) for 63 HNNs, each using a different combination of training data (i.e., soil profiles) and environmental variables. The HNNs trained to four or five soil profiles that used a subset of t, T, Q, E, and A as predictor variables yielded lower MSEs than the PBM, and showed global convergence. At least two variables are needed to achieve an MSE within 1% of the corresponding PBM. The HNNs generally predicted the slope better than the depth of the front because the PBM was not used to predict depth. HNN results identify t and P as the most and least useful variable in predicting the reaction front, respectively. This is the first time a NN was hybridized to a PBM to simulate reactions in soils. As part of this effort, we developed a tool to identify cases which have converged to a global solution, and cases which present local solutions. The approach shows promise for future efforts but should be applied to larger sets of soil profile data and PBMs that predict both the depth and slope of reaction fronts.

1. Introduction

Recent improvements in data-driven modeling have opened up new avenues to assess Earth and environmental science data (Bergen et al., 2019; Shen et al., 2018; Shen, 2018). However, this approach has yet to show utility in identifying natural laws from observational data (Schmidt and Lipson, 2009) and is generally not used in hypothesis testing (Shen, 2018). One promising new avenue is the integration of data-driven techniques with physics-based models (PBM).

In soils, dissolution reaction fronts are localized zones of weathering in areas of generally downward-flowing water that appear as depth intervals where one mineral dissolves and is removed from the soil as a solute while another mineral may be precipitated (e.g., Brantley and White, 2009; Lichtner, 1988). Reaction fronts can reveal the flow of meteoric water in the subsurface over geologic time periods (Brantley et al., 2017) and may indicate geological rates of CO_2 removal from the atmosphere by natural long-term processes (Godderis et al., 2019). Researchers have developed and adopted a variety of PBMs, e.g., reactive transport models (RTM), to reconstruct reaction fronts in soils (e.g., Godderis et al., 2019; Li et al., 2017; Maher and Navarre-Sitchler, 2019; White et al., 2001). These models require RTM codes that treat transport of solutes in flowing water (advection), transport of solutes through the

---

* Corresponding author.
  E-mail address: twen08@syr.edu (T. Wen).
[1] These authors contributed equally to this work.

water in the soil and rock pores (diffusion), and chemical reactions between solutes and the soil grains (e.g., Lebedeva et al., 2007; Li et al., 2017; Lichtner et al., 1996). Although RTMs are becoming increasingly useful to predict changes in aqueous and solid-phase chemistry over space and time, they are often difficult to parameterize because of the lack of data for and prior knowledge of the environmental, thermodynamic, and kinetic conditions of the associated system (e.g., Moore et al., 2012). Researchers therefore generally rely on uncertainty propagation, sensitivity testing (both local and global) of parameters, and calibration to evaluate the importance of the many required but generally unconstrained or loosely constrained parameters (Laloy and Jacques, 2019). To ascertain the uncertainty of the model prediction accurately can require thousands to tens of thousands of simulations.

Several published papers have explored the use of neural networks (NN) to simulate aspects of soil-water evolution. One such recent effort was to determine dispersivity and retardation factors of solutes in waters infiltrating soils (Mojid et al., 2019). Another team trained a NN to a reactive transport simulation of a geochemical system considered at microscopic scale and then successfully used it within a model of a macroscopic system (Prasianakis et al., 2020). Another research effort attempted to use a NN as an emulator model in comparison to a complete reactive transport model (Laloy and Jacques, 2019).

Here, we focus on solid-phase chemical and mineralogical profiles in regolith over space and time. These solid-phase datasets document the long-time interaction of soil materials and meteoric waters. Generally when using reactive transport models to simulate the changes in soil materials during weathering, we often start with a known depth profile of soil/rock composition, the change of which over long time periods due to weathering is dictated by infiltration and percolation of recharge water through the soil profile (e.g., Moore et al., 2012). In this study, we did not seek to simulate this full complexity of processes. Rather, we tried to take a small first step in developing a NN for use in predicting reaction fronts in soils. We sought specifically to minimize model discrepancy between a PBM that had been previously proposed to describe a single reaction front in a soil column (Brantley et al., 2008) and predictions from the use of NNs. Note, this simplified PBM is ultimately a sigmoidal function fitted to the sodium concentration in solid-phase soil across depth. We attempted to develop a hybrid neural network (HNN) that incorporates the NN and this PBM to explore whether NNs can be used to improve the accuracy of physics-based modeling results and whether we can extrapolate findings from one location to another. We trained the HNN with soil data included in the training data and then tested the trained model against data from other soil profiles contained in the testing data. We sought to determine if the HNN was able to (1) simulate soil profiles that were not part of the training data but had formed in a similar climate and erosional regime like the soils in the training data; (2) simulate soil profiles that were not part of the training data and had formed in different climates; and (3) simulate soil profiles that were not part of the training data and had formed in different erosional regimes. Our approach differs from the previous NN efforts in that we focus on the solid-phase chemistry in water-rock reaction systems which represent the integrated results of weathering processes over a longer timescale compared to the solute chemistry. In addition, unlike the PBM which requires domain knowledge of every single simulated soil profile for the model parameterization, our proposed HNN can potentially extrapolate the knowledge (i.e., trained HNN) learned from one or more soil profiles to the other (i.e., predictions using the trained HNN). We anticipate that such HNNs could eventually become of great help to simulate soil profiles without the need of prior domain knowledge.

2. Theoretical background

2.1. Soil profiles

We first compiled soil chemistry data from a few soil profiles that

have formed as meteoric water infiltrates parent material over geologically long periods of weathering (e.g., Brantley and Lebedeva, 2011). We model the soils as one-dimensional systems where the parent material (rock or sediment) is exposed and can be affected by erosional processes that may remove material from the land surface while meteoric water infiltrates, on net, unidirectionally downward. Over time, minerals dissolve and precipitate in the soil column. Therefore, the abundances of different minerals vary with depth over time. Multiple minerals that have different solubility exist in soil and rock. For example, rocks commonly contain quartz (mostly insoluble) plus feldspar (soluble). Thus, in many soils, feldspar weathers to precipitate a clay such as kaolinite (insoluble) while the quartz remains unweathered, propping open the porosity and holding the overall volume of the weathering material constant (isovolumetric weathering). Feldspar contains the common element sodium (Na), but kaolinite does not contain Na. Therefore, weathering of a rock column (that includes feldspar + quartz) yields a column with decreasing concentrations of Na near the land surface. Na is removed from the soil layers as kaolinite is precipitated until the Na concentration (and by inference, feldspar) reaches zero at the land surface. At that point, the soil at the land surface is strictly quartz + kaolinite. The depth interval over which Na concentration varies from zero to the abundance in the parent material is called the interval of the reaction front. In some soils, the reaction front can be overlain by a depth interval that lacks feldspar, if the reaction front has advanced and no longer truncates the land surface.

As rock material weathers to soil, it can lose mass not only by (bio) geochemical weathering (e.g., dissolution) but also at the land surface, by physical losses known as erosion (Riebe et al., 2016). While weathering of a rock column (that includes feldspar + quartz) yields a column with decreasing concentrations of Na towards the land surface, erosion can remove the topsoil. Regardless of whether a soil is eroding or not eroding, the depth profile of Na concentration can generally be used to indicate the feldspar reaction front. More details of soil weathering can be found in the supplementary text ("Theoretical background of Soil Weathering").

2.2. Physics-based modeling of soil profiles

A full implementation of a reactive transport model to simulate soil weathering requires many parameters that are often unknown. Moreover, the choice of those parameter values to ensure a successful model simulation is often non-unique. This property of equifinality is common to a wide variety of Earth and environmental science models (Shen, 2018) including hydrologic models (Beven and Freer, 2001), models of global biogeochemical cycling (Tang and Zhuang, 2008), reaction kinetics (Bandstra and Tratnyek, 2004), and water quality models (Schulz et al., 1999). In many of these cases it is possible to formulate relatively simple empirical relations that describe biogeochemical processes on an average basis over sufficiently large spatial or temporal scales (Savenije, 2001). Such models have the advantage of being parsimonious and capable of describing the relevant phenomena under a broad range of environmental conditions but with the drawback of parameter values that are *sui generis* and that must be estimated from data (e.g., by regression analysis). This modeling approach is referred to as physics-based modeling or PBM as illustrated in Fig. 1a.

Brantley et al. (2008) proposed a parsimonious PBM for soil profiles that accounts for the opening of reactive surface area as the parent material first begins to weather leading to eventual depletion of non-conservative elements (such as Na) as the weathering process moves toward completion. Brantley et al. (2008) showed that under a generalized set of assumptions, the soil profile can be modeled as the reaction front of an autocatalytic process, i.e., a sigmoidal curve of the form:
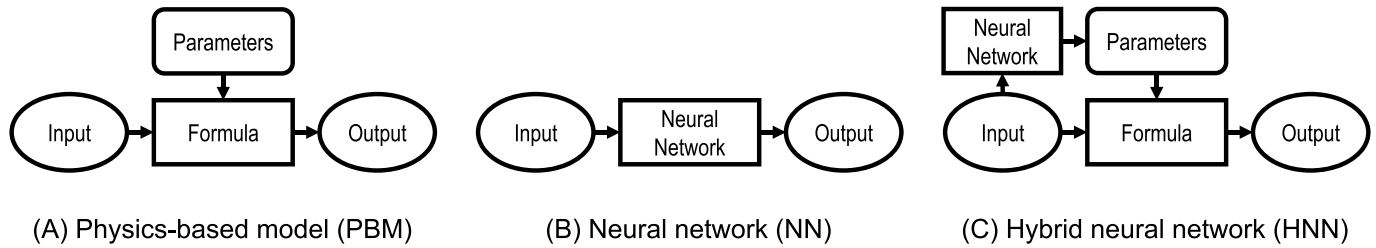
Fig. 1. Conceptual illustration for (A) physics-based model or PBM, (B) neural network or NN, and (C) hybrid neural network or HNN. The PBM develops an equation (central box labelled "formula") to predict output values (y) from input value(s) (x) for physical or chemical processes. This formula is based on physical observations and reflects physics-based laws. Thus, a PBM provides an equation with parameters where the parameters (here, $\Gamma\_ini·\hat{k}\bar{\ }$) in the formula are thought to be explained by known observable phenomena. These parameters may change as a function of properties of the environment where the data samples are collected. In contrast, the NN directly learns the function that links the input and output. A HNN uses both the PBM and the NN to learn the appropriate parameters.

$$C = \frac{C_0}{\frac{C_0 - C_{x=0}}{C_{x=0}} \exp(\Gamma_{ini} \cdot \hat{k} \cdot x) + 1} \tag{1}$$

where C is the concentration, or abundance (mol/m^3), of an element such as Na in a soil profile at a given depth x below the land surface, Γ_{ini} describes the roughness of the surface area of the dissolving mineral, and $\hat{k}$ is a lumped kinetic parameter that describes the reactivity of the mineral and its initial specific surface area. $C_{x=0}$ is the concentration (abundance) of the element at the land surface ($x = 0$), or, for a reaction front that has advanced into the subsurface, at the top of the front. C_0 is the concentration of the element in the underlying (unweathered) parent material.

Eqn. (1), when applied as a non-linear regression equation, suitably describes soil profiles developed on several different parent materials, under different climate conditions, and with different geomorphic time-scales (Brantley et al., 2008). Each soil profile, however, requires a unique set of parameter values and, therefore, Eqn. (1) lacks predictive power for soil profiles developed under novel conditions. To overcome this limitation, we sought to leverage the power of NN to develop an HNN that could similarly simulate the depth profile of Na content in the soil after long duration weathering. Although this PBM is not nearly as powerful as an RTM, our attempt to develop an HNN using this PBM represents a first step in the direction of ultimately hybridizing with RTMs. Furthermore, the equation implicitly reveals the reaction front thickness – an observable that can provide information related to the advective Damköhler number for the reactive transport system in some soils (Brantley and Lebedeva, 2021).

2.3. Hybridization of the physics-based model with an artificial neural network

Artificial neural networks (ANNs) represent a group of widely-used machine learning models (Fig. 1b) that can show superior performance in regression fitting problems (Goodfellow et al., 2016; LeCun et al., 2015). Typically, these models are described as a stack of layers consisting of an input layer, at least one hidden layer of neurons, and an output layer. The input layer corresponds to the independent (or predictor) variable(s) in the regression analysis while the output layer corresponds to the dependent (or target) variable.

Each hidden layer in ANNs consists of several neurons and the input to each neuron is a linear combination of the outputs from the previous layer as specified by a vector of weights W and a bias b, i.e., activation function [Eqn. (2)]. Note that the activation function could be set as non-linear (e.g., sigmoid).

$$h_{i,j} = \sigma\left(\overrightarrow{W}_{i,j} \cdot \overrightarrow{h}_{i-1} + b_{i,j}\right) \tag{2}$$

Here, i denotes the i-th layer and j denotes the j-th neuron within the layer. For the j-th neuron in the i-th layer ($\overrightarrow{h}_{i,j}$), the output of this neuron

is the bias scalar $b_{i,j}$ plus the weighted sum of input neurons from the previous layer, $\overrightarrow{h}_{i-1}$ (the vector of weights is $\overrightarrow{W}_{i,j}$). The vector length in Eqn. (2) is determined by the previous layer while the maximum of indices i and j are hyperparameters defined by the user. ANN containing multiple hidden layers is able to approximate arbitrarily complicated functions (Cybenko, 1989; Hornik, 1991), a property known as universality.

Although universality is a useful property when it comes to fitting variable phenomena, it is a limiting factor for their direct use in scientific discovery (Brouwer et al., 2014; Livingstone et al., 1997). In a manner analogous to equifinality in PBMs, universality implies that many ANNs can be constructed to adequately capture the state of knowledge about a natural phenomenon. While this does not limit the use of ANNs in forecasting, it does limit the use of ANNs for extracting principles or testing hypotheses. To overcome this limitation, NNs are now being hybridized with PBMs to learn new scientific concepts from observational data (Karpatne et al., 2017).

An HNN (Fig. 1c) combines a PBM and a NN. Different from the NN itself, the output of the HNN is still governed by the physical formula. In the HNN, a NN is used to find the optimal values of parameters (e.g., environmental variables) in the formula by modeling and minimizing the mismatch between prediction results from the PBM and the observations. For the example here, the HNN predicts the term, $\Gamma_{ini} \cdot \hat{k}$, in Eqn. (1) by using site climate characteristics, geomorphic rates, and parent mineral composition as the input layer to an ANN. Specifically, we assess how the term, $\Gamma_{ini} \cdot \hat{k}$, varies with the residence time and quartz content of the soil, the erosion rate, temperature and precipitation rate of the soil site, and the composition of the feldspar observed in the targeted reaction front.

The PBM was derived (Brantley et al., 2008) to describe a generic feldspar reaction front in soil (e.g., Brantley and White, 2009), in which the proposed formula, Eqn. (1), has only been used to fit individual soils. The parameter for surface area and kinetic reactivity [$\Gamma_{ini} \cdot \hat{k}$ in Eqn. (1)] is a function of not only soil depth x but also the residence time of particles in the soil and other factors as further discussed later. In this work, we explore how the value of $\Gamma_{ini} \cdot \hat{k}$, which is implicitly related to the advective Damköhler number for reactive transport in some soils (Brantley and Lebedeva, 2021), varies with environmental conditions and parent material characteristics. Specifically, previous works have shown that soil/rock weathering is affected by a set of soil-forming factors related to climate, biota, relief, parent material, and time (Dokuchaev, 1883; Jenny, 1941; Merrill, 1906). Thus, variations in the value of $\Gamma_{ini} \cdot \hat{k}$ could be affected by a combination of variables such as soil residence time or exposure time (t), mean annual temperature (T), erosion rate (E), and/or precipitation rate (P), and so on. Given that $\hat{k}$ includes the rate constant of feldspar dissolution, and this is known to vary with the albite content (A) of the dominant feldspar in the parent material (Blum and Stillings, 1995), we also sought to understand if the sodium (Na) content of the feldspar (equivalent to albite content)

controls the characteristics of the reaction front. Finally, we also aimed to test the hypothesis that the quartz content (Q) of the starting material might also affect the depth of the reaction front as suggested by reactive transport models (Brantley et al., 2017). These are all specific tests that we chose to pursue within our overall goal of exploring how to use a NN with a PBM for soil modelling.

To formulate the HNN, we defined $f(z) = \Gamma_{ini} \cdot \hat{k}$, where z represents any combination of predictor variables, e.g., $f(t)$, $f(t, T)$, $f(P, E)$. $f(z)$ is a NN consisting of one input layer, two fully connected hidden layers [Eqn. (2)], and one output layer [Eqn. (3)]. The activation function of the first hidden layer is a sigmoidal function [Eqn. (4)] while the activation function of the second hidden layer is the simple linear combination of all input neuron results. The output of the second fully connected layer is not determined by an activation function but rather by the PBM as shown in the equation below that is modified from Eqn. (1).

$$C' = \frac{1}{\frac{C_0 - C_{x=0}}{C_{x=0}} \exp(f(z) \cdot x) + 1} \qquad (3)$$

$$\sigma(z) = \frac{1}{1 + e^{-z}} \qquad (4)$$

where we have normalized Eqn. (1) by the parent concentration C_0, i.e., $C' = \frac{C}{C_0}$. Eqn. (3) represents the HNN which incorporates a data-driven model into a physics model. The HNN is guided by the physics law that governs the PBM, while the lumped rate parameter, $\Gamma_{ini} \cdot \hat{k}$, is inferred from data using a NN.

3. Computational methods

3.1. Soil datasets

Seven soil profiles were compiled from four sites in the U.S.: Santa Cruz (California; four soil profiles: SCT1,2,3,5; Fig. 2), Davis Run (Virginia), Panola (Georgia), and Jughandle State Natural Reserve (California) (Table 1 and S1). Except for the Jughandle soil profile, all other soil data were previously investigated (Brantley et al., 2008, 2017, 2008; Brimhall and Dietrich, 1987; Eckert et al., 2012; Maher et al., 2009; Masiello et al., 2004; Merritts and Bull, 1989; Merritts et al., 1991; Moore et al., 2012; Northup et al., 1995; Uroz et al., 2014; White et al., 2001, 2008, 2009). Detailed description of these soil profiles can be
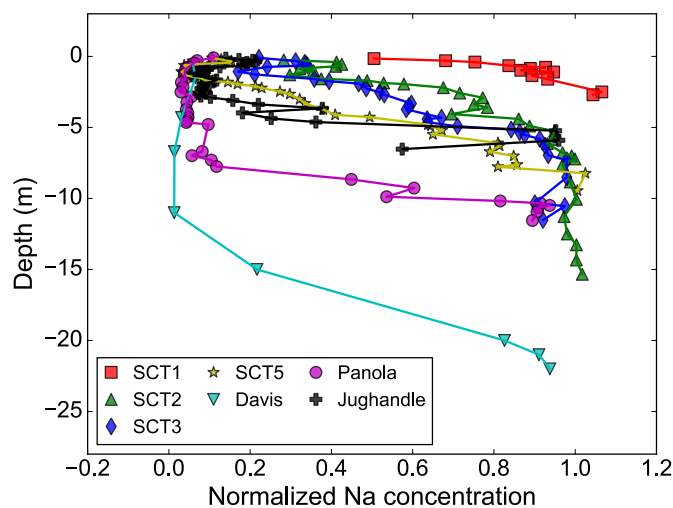

Fig. 2. Depth profiles of normalized Na concentration in the seven soil profiles discussed in this study. All Na concentrations are divided by that of the corresponding parent material.

found in the supplementary text "Detailed Descriptions of Soil Datasets". Sodium concentrations in the solid phases of these soils from these seven profiles were normalized by the sodium concentration in the corresponding parent material (underlying unweathered material) before being fed into the neural network. Normalized sodium concentration mostly varied from 0 to 1. Predictor variables were not rescaled due to two primary reasons: 1) our NN is a two-layer dense neural network that should be capable of learning to scale the variables itself without the need of manual preprocessing (Hornik et al., 1989); 2) we also sought to derive the mathematical formula from the HNN that we can apply to calculate the lumped parameters of the PBM. The data preprocessing without the rescaling allows the direct derivation of such mathematical formula from the HNN.

3.2. Model setup and model training

Based on knowledge from soils research and modeling (Brantley et al., 2017; Lebedeva et al., 2010), we hypothesized that residence time (t), temperature (T), precipitation (P), erosion rate (E), quartz content (Q), and the albite content of the feldspar in the parent material (A) could explain differences in the reaction fronts in different soils. We thus used t, T, P, E, Q, and A as predictor variables in the HNN. Measurements of predictor variables were not scaled while Na concentrations were normalized by the Na concentration in the parent material. In total, an HNN was trained and constructed for each of the 63 different combinations of predictor variables. In every case, $C_x = 0$ and C_o (Table 1) were treated as known quantities. Full results of the training and test phases for each of the 63 HNNs are summarized in Table S2. Although we did not perform feature selection in this study since the selection of all the six features was already parsimonious and the computational cost was not an issue for the proposed simple HNN, it might be necessary to perform feature selection if the proposed HNN would be used to simulate other soil profiles using a lot more features from the perspective of computational efficiency.

Models were trained with three different sets of soil profiles: (SCT1, SCT 2, SCT 3, SCT 5, Panola) or (SCT1, SCT 2, SCT 3, SCT 5, Davis Run) or (SCT1, SCT 2, SCT 3, SCT 5) when possible (Table S2). Models using these training sets were labelled a, b, and c, respectively. For variables such as residence time t where every soil was characterized by a different value, i.e., the investigated soils all differed in estimated residence times, the model (e.g., in this case f(t)) was trained with all three sets. But for other variables such as T where subsets of soils displayed the same value(s) for predictor variable(s) (e.g., SCT1, 2, 3, 5 all have the same temperature T), models were not trained with all three sets of soils (a, b, c). For this example, f(T) was only trained with a and b sets. Given this, only a subset models of f(t), f(Q), f(A), f(t,Q), f(t,A), f(Q,A), and f(t, Q,A) were trained with training set c and then used to predict the other three non-chronosequence (non-SCT) soils.

Optimized weights and biases were found for the NN component of the HNN by minimizing mean square error (MSE) between the HNN output and the normalized measured Na concentration data. MSE was chosen to measure the model performance because it reflects the discrepancy between model prediction and observational results. The Adam method (Kingma and Ba, 2014) was used for stochastic optimization with a learning rate of 0.001. The optimization was terminated after 15,000 steps, upon which all our models converged (i.e., MSE stopped decreasing significantly).

The first hidden layer of 16 neurons was used with a sigmoid activation function. The second hidden layer has 1 neuron with linear activation. We performed a grid search to determine the best number of neurons based on MSE. For the number of neurons in the first layer, we tested 8, 16, 32 while 1 and 2 were tested for the hyperparameter of the number of neurons in the second layer. Another hyperparameter – the number of hidden layers – was also fined tuned by testing values of 1 and 2. Given the extremely small number of layers (i.e., two) of the NN and the small number of features (i.e., at most six), this simple structured

Table 1
Summary of parameters describing soils.[a]

Name	Residence time (t, ky)	Temperature (T, °C)	Erosion rate (E, m/My)	Precipitation (P, mm/y)	Quartz content (Q, vol %)	Fraction of Na feldspar in parent feldspar (A)	C_0 (mol/m[c])
SCT1	65	13.4	0	727	27.17[e]	0.66	1560[f]
SCT2	90	13.4	0	727	23.25[e]	0.73	1380[f]
SCT3	137	13.4	0	727	25.36[e]	0.72	1250[f]
SCT5	226	13.4	0	727	34.08[e]	0.70	1320[f]
Davis	2500[2]	10	4	1040	36.3	0.94	2500[f]
Panola	1714[b]	17	7	1240	27.5	0.77	3020[f]
Jughandle[d]	500	12.5	0[c]	983	34.08[c]	0.70[c]	656[g]

[a] Values were derived from White et al. (2008) and White et al. (2001) [for summary see also Brantley et al. (2008)] unless noted otherwise.

[b] These times were calculated by assuming an erosion rate of 8 m/My or 7m My and the regolith thickness of 20 m and 12 m for Davis Run and Panola soils, respectively, for the residence time of minerals in the regolith depth interval assuming steady-state thickness, i.e., the soil residence time. These erosion rate and regolith thickness values were reported in the literature (Bierman et al., 1995; Pavich, 1986; Pavich et al., 1985; White et al., 2001).

[c] Assumed the same as SCT5.

[d] Climate values from (Northup et al., 1995) and residence time estimated from (Merritts and Bull, 1989).

[e] Calculated as vol. % based on data reported in White et al. (2008) and Brantley et al. (2008).

[f] Best model fits from Brantley et al. (2008).

[g] Best PBM model fits performed in this study.

neural network model is very unlikely to overfit. In particular, for those best-performing HNNs (see Section 4.2), each of them considers only two features, which renders it less likely for them to overfit.

3.3. Regression analysis with physics-based models

Parameters in the PBM – C_0, $C_{x=0}$, and $\Gamma_{ini} \cdot \widehat{k}$ – were selected to fit each soil profile by minimizing the chi-squared statistic (χ^2). χ^2 is the sum-of-square errors between Eqn. (1) and the measured Na concentrations normalized by the variance of the residuals. For an individual soil profile, χ^2 is directly proportional to the MSE as discussed below. χ^2 was minimized using the Levenberg-Marquardt algorithm (as implemented in Igor Pro 8 from Wavemetrics Inc.) with a termination criterion of nine iterations with no more than a 0.1% decrease in χ^2 (Press et al., 2007). Initial guesses for the parameters were determined by visually estimating (1) the concentration of Na in the parent material, (2) the slope of the soil profile at its inflection point, and (3) the depth of the inflection point. The initial guess for C_0 was taken directly from the estimated parent concentration. Initial guesses for the other two parameters were calculated as:

$$\Gamma_{ini}k \approx \frac{4}{C_0}\left|\frac{dC}{dx}\right|_{IP}$$ (5)

$$C_{x=0} \approx \frac{C_0}{1 + \exp\left(\Gamma_{ini}k|x|_{IP}\right)}$$ (6)

where the subscript IP denotes values estimated at the soil profile inflection point.

In several cases, we followed standard practice and excluded a few near-surface concentration data points from the fits owing to apparent exogenous disturbance (i.e., dust inputs). These near-surface soils were perturbed by eolian input and bioturbation, which interfered with the pristine signatures of soil development over time (Brantley et al., 2008). Data excluded from fitting were the first 2 m of the ~10-m-deep Panola granite profile, the first 5 m of the ~22-m-deep Davis Run profile, and the first meter of the ~6-m deep Jughandle profile.

4. Results and discussion

4.1. Training phase of the hybrid neural network

MSE values for the HNN results for all seven soil profiles ranged from 0.0030 to 0.38 with an average MSE of 0.072 (Table S2). Below, we compare the HNN MSE values with the corresponding PBM MSE values by calculating the percent difference between these two MSE values as

follows:

$$\text{Percent difference in MSE} = \frac{MSE_{HNN} - MSE_{PBM}}{MSE_{HNN}}$$ (7)

In some cases, the HNN was able to achieve slightly lower MSE than the PBM (see Table S2) but in all such cases, the difference in MSE was likely due to rounding of the PBM parameters as previously reported (Brantley et al., 2008). For visualization purposes, these negative percent differences were set to 0.1% in Figs. 3, 4 and 6. This value effectively identifies these cases as ones where the HNN was able to precisely reproduce the PBM.

In other cases, the HNN underperformed the PBM. This could be due to HNNs that converged to local minima in MSE instead of the global minima or it could be due to an inadequate set of predictor variables. A methodology for identifying cases of local convergence is developed in Section 4.1.1. In Sections 4.1.2 and 4.1.3 we assess how the number of predictor variables controlled the prediction accuracy of HNNs as well as
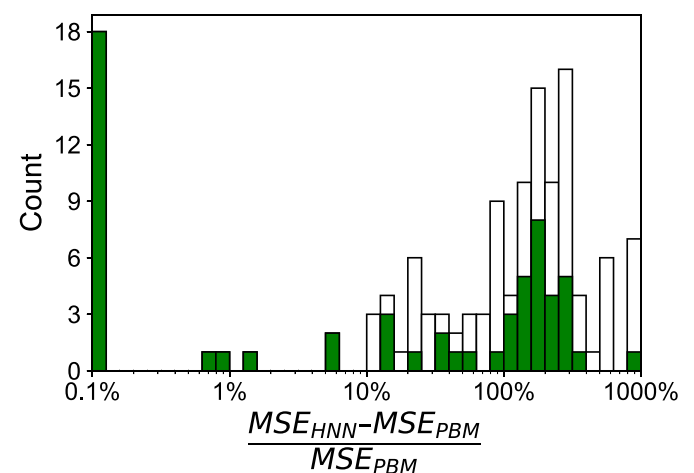

Fig. 3. Histogram of percent difference in MSE between HNNs and their corresponding PBMs in the training phase. All negative percent difference values were set to 0.1% for visualization purposes. The unshaded portion of the histogram represents those HNNs that used a subset of predictor variables and yielded MSE values that were 10% larger than that of at least one HNN. We inferred that these HNNs very likely converged to local minima instead of a global optimum. The green shaded portion represents those HNNs with MSE within 10% of that of any HNNs that use a subset of predictor variables. These HNNs were considered to have been more likely to converge to the global minima. (For interpretation of the references to colour in this figure legend, the reader is referred to the Web version of this article.)
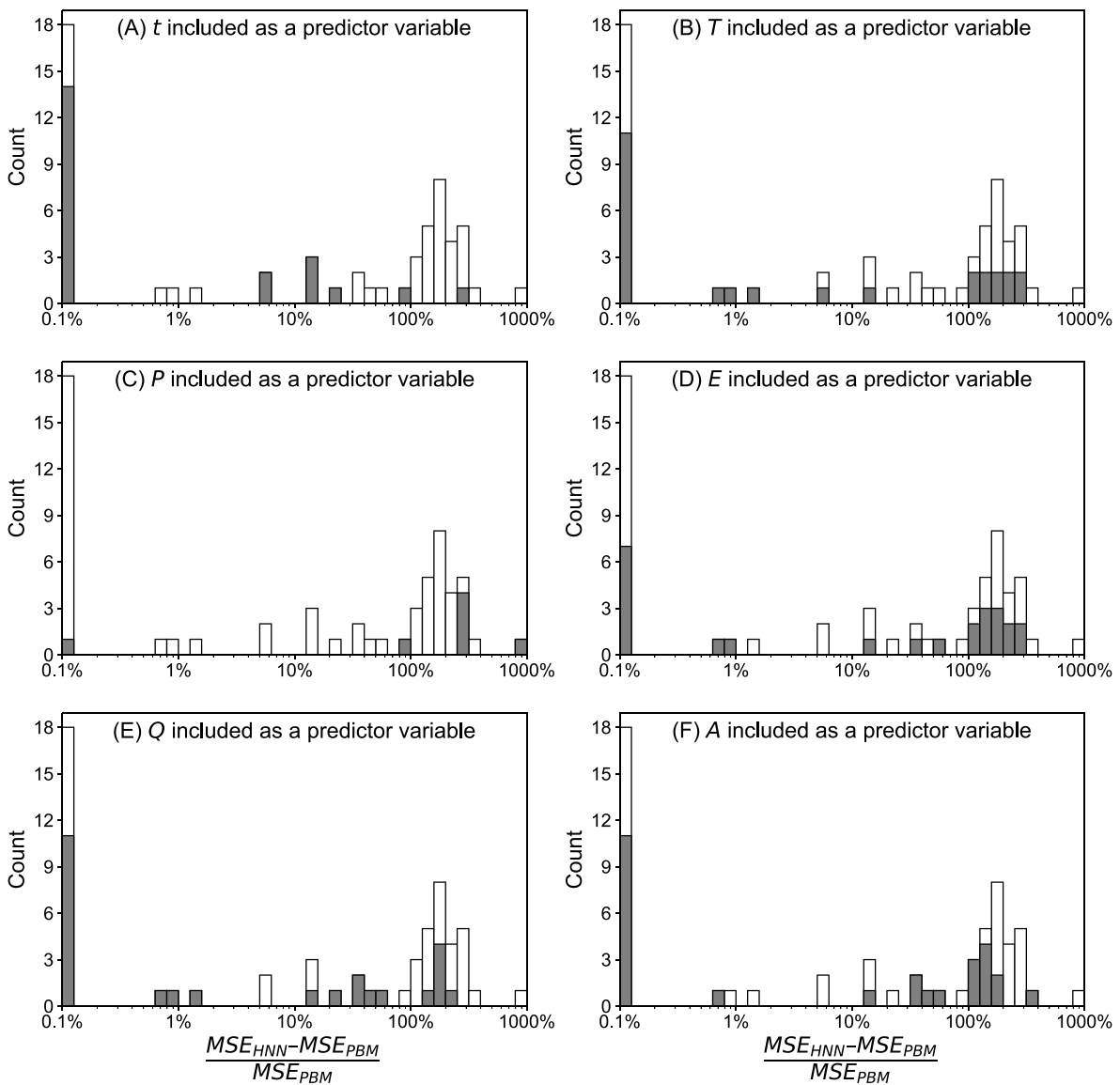
Fig. 4. Histogram of percent differences in MSE between HNNs and their corresponding PBMs in the training phase (local-converged HNNs excluded). All negative percent differences were set to 0.1% for visualization purposes. The shaded portion represent those HNNs that include (A) soil residence time/exposure time or t, (B) temperature or T, (C) precipitation or P, (D) erosion rate or E, (E) quartz content or Q, and (F) albite content of the feldspar or A as one of the predictor variables.

which predictor variable(s) might be the most important environmental factor dictating the development of reaction front in the soil profile.

4.1.1. Local convergence in the hybrid neural network

The percent difference in MSE between HNNs and their corresponding PBMs in the training phase was calculated by following Eqn. (7) and is plotted as a histogram in Fig. 3. A total of 26 HNNs (out of 63) reported a MSE less than 10% of that of the corresponding PBM, indicating a comparable prediction performance between the HNN and PBM in the training phase for these 26 HNNs.

For any given HNN we define a subset HNN as one that was trained with the same data but using only a subset of the same predictor variables. For instance, HNN 22a was trained on SCT1,2,3,5 and Panola data using t, T, and P as predictor variables. HNN 7a was trained on those same data with t and T as predictor variables. Therefore, in our terminology, HNN 7a is a subset HNN to HNN 22a.

If an HNN and all of its subset HNNs have converged each to their global minimum in MSE, then the parent HNN should perform no worse in terms of MSE than any of its subset HNNs. Of course, the parent HNN could outperform one or more of its subset HNNs but the reverse cannot

occur. Because the HNN parameterization methods are stochastic, some allowance for slight and insignificant outperformance must be made, but we observed a number of cases where an HNN was outperformed by one of its subset HNNs by more than 10% (i.e., the MSE for the parent was greater than 1.1 times the MSE for the subset HNN), which are defined as locally-converged HNNs. Otherwise, HNNs are named as globally-converged HNNs.

In Fig. 3, those HNNs that were not significantly outperformed (at a level of 10%) by any subset HNN have been shaded green. These HNNs have likely converged to a global minimum. A characteristic feature of these apparently well converged HNNs is that they tended to use a larger number of predictor variables (see Section 4.1.3). In contrast, we also found many HNNs with MSE 10% larger than that of at least one subset HNN, suggesting convergence to a local minimum in MSE, i.e., local convergence. This latter circumstance could lead to the conclusion that additional predictor variables lowered the MSE of the HNN. In the following discussion, we excluded all these locally-converged HNNs, and only considered those HNNs more likely to have converged to the global minima (shaded green in Fig. 3).

4.1.2. Hybrid neural network and predictor variables

As discussed in the text above, six predictive factors were considered: climate characteristics (temperature T and precipitation P), geomorphic parameters (soil residence time or exposure time t and erosion rate E), and parent material mineralogy (quartz abundance in the soil Q and albite content in the feldspar A). We explored the relative importance of all the six predictor variables in the HNN by assessing which predictor variable was most frequently included in the best performing HNNs.

Fig. 4 summarizes the number of HNNs (excluding those likely locally converged) that includes each of the six predictor variables. Among those HNNs within 10% of the MSE reported by the corresponding PBM, t, T, P, E, Q, and A were used in 16, 15, 1, 9, 14, and 12 HNNs, respectively. For those HNN with a percent difference in MSE of less than 0.1%, 14, 11, 1, 7, 11, and 11 HNNs included t, T, P, E, Q, and A, respectively.

These results suggested that soil residence time or exposure time (t) is the most useful predictor variable for parameterizing an HNN that can reproduce the behavior of the PBM with respect to slope of the reaction front. Temperature (T), erosion rate (E), and albite content of the feldspar (A) are also helpful predictors while the precipitation (P) was the least useful predictor variable.

The HNN ultimately predicted the parameter of $\Gamma_{ini} \cdot \widehat{k}$ in the PBM (Eqn. (1)) using a data-driven approach, and yielded the derived value of $\Gamma_{ini} \cdot \widehat{k}$ as the function – f(z). To further illustrate how the derived f(z) varied with the soil residence time or exposure time (t), the most useful predictor variable, and how it compared to the $\Gamma_{ini} \cdot \widehat{k}$ in the PBM, we inspect the prediction results of HNN model 1c f(t) (Fig. 5). HNN model 1c was trained to soil profiles SCT1, 2, 3, and 5. As shown in Fig. 5, the derived f(z) value from the HNN and $\Gamma_{ini} \cdot \widehat{k}$ from the corresponding PBM were very similar. In addition, the derived f(z) varied significantly with the soil residence time or exposure time. As the soil residence time or exposure time increased in the order of SCT1, 2, 3, and 5, f(z) first decreased and then increased before reaching a plateau.

4.1.3. Hybrid neural network and number of predictor variables

We then explored how the number of predictor variables included in the HNN contributed to the improvement of HNN performance (i.e.,
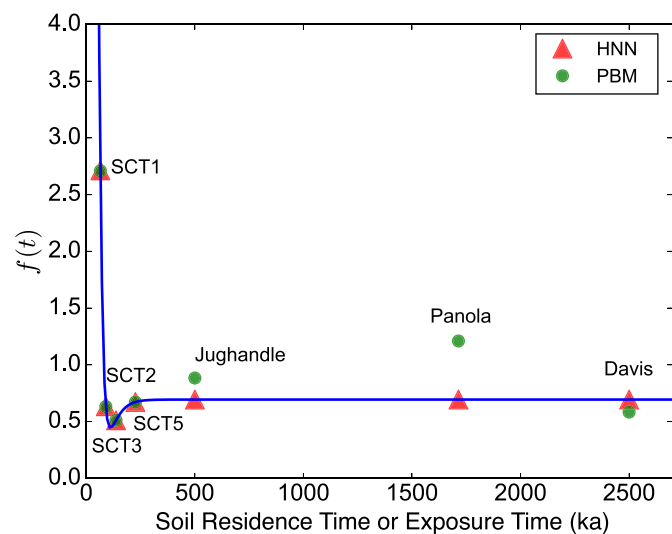

Fig. 5. Plot showing *f(z)* predicted by HNN 1c *f(t)* (red triangles) as a function of the soil residence time. $\Gamma_{ini} \cdot \widehat{k}$ values derived from the corresponding PBM are also shown for each soil profile (green circles). Blue curve calculated from the function *f(t)* given by HNN 1c is plotted to illustrate how the *f(z)* value varies with the soil residence time in the HNN 1c. (For interpretation of the references to colour in this figure legend, the reader is referred to the Web version of this article.)

lowering of the MSE value).

Fig. 6A plots the percent difference in MSE between the HNN and the corresponding PBM as a function of the number of predictor variables included in the HNN. The improvement in the MSE was significant from the HNN using one predictor variable to the HNN using two predictor variables. At best, HNNs with only one predictor variable could only achieve MSE values within 10% of the corresponding PBM. At least two predictor variables were needed to construct an HNN that achieves an MSE within 1% of the corresponding PBM. Adding additional predictor variables beyond two was not significantly advantageous.

Among those globally-converged HNNs, a total of 23 HNNs report MSE values within 10% different from that of the corresponding PBM. Among these were seven HNNs that include two predictor variables (Fig. 6B and Table 2). These seven HNNs that use only two predictor variables are defined as the best performing HNNs in this study, and are further discussed below.

4.2. Best performing hybrid neural network models

MSE values of the seven best performing HNNs in the training and test phases, and the MSE values of the corresponding PBMs were listed in Table 2. To reiterate, a best-performing HNN is defined as (1) the HNN attained an MSE no more than 10% worse than any subset HNN in the training phase and (2) the HNN attained an MSE value within 10% of the corresponding PBM on the same training soil profiles.

The predictor variable of residence or exposure time of the soil (t) was included in all but two of the best performing HNNs. This emphasizes again that residence or exposure time is the most useful variable in predicting the slope of the reaction front using the HNN (see, for example, Fig. 5). Many researchers have previously emphasized the importance of residence time or exposure time on reactivity (Washton et al., 2008; White and Brantley, 2003), and by inference, on the slope or thickness of the reaction front. In contrast, precipitation is the least useful predictor variable. This latter insight from the HNN work was surprising from a physics point of view. The HNN is mostly predicting the slope of the reaction front (see discussion below), and the slope is a function of the infiltration velocity of meteoric water into the soil, the reaction rate constant, the mineral surface area available for dissolution, and the abundance of the reacting mineral (Brantley and White, 2009). Apparently, although the precipitation P at the land surface is a boundary condition for the infiltration velocity, the velocity at the depth of the reaction front is more of a function of residence time or exposure time than the climate variable P, at least for this subset of soils developed in moderately rainy conditions. This could be related to many complicating factors related to evapotranspiration, biotic activity, plant succession, plant physiology, soil nutrient content, and climate. In addition, as a soil profile develops, water that initially infiltrates vertically and reacts with minerals begins to flow laterally, especially at reaction fronts (Brantley and Lebedeva, 2021). With lateral flow, less downward-advecting water percolates through the deepening reaction front as soil layers develop and differentiate. This in turn affects the slope of the reaction front. The finding from the HNN is novel in that it emphasizes the importance of t and de-emphasizes the importance of P in determining the slopes of reaction fronts in field settings.

Among these seven HNNs, four models (i.e., 7a, 9a, 11a, 14a) were trained to SCT1,2,3,5 and Panola soil profiles ("a" series training set). Two models (i.e., 7b, 14b) were trained to SCT1,2,3,5 and Davis soil profiles ("b" series training set) while one model (i.e., 11c) was trained to only SCT1,2,3,5 soil profiles ("c" series training set). In particular, both f(t,T) and f(T,Q) were able to train successfully with "a" and "b" series training sets (7a and 7b, and 14a and 14b), while f(t,A) was able to train successfully with "a" and "c" series training sets (11a and 11c). Model f(t,T) was not trained with the "c" series training set because the temperature (T) did not vary across the soil profiles of SCT1,2,3,5 and f(t,T) therefore could not be calculated for the "c" series training set. Due to the same reason, f(T,Q) was not trained with the "c" series training
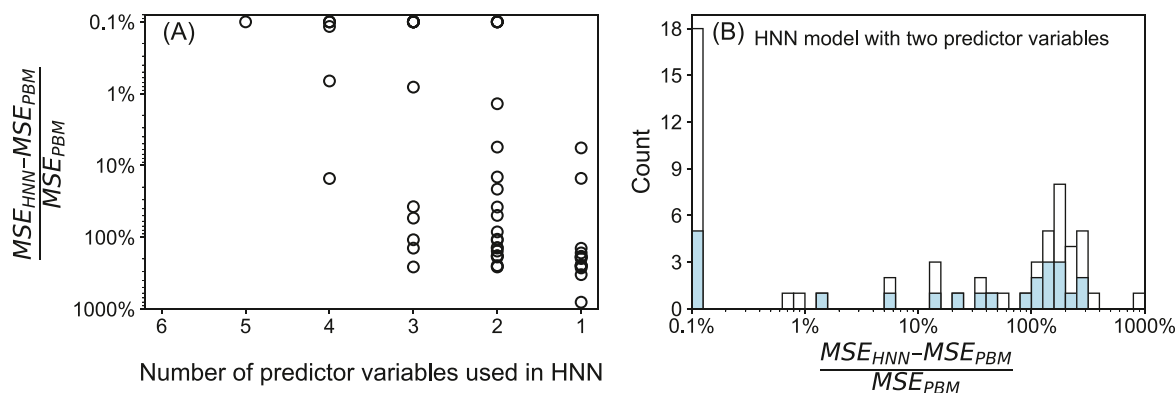
Fig. 6. (A) Plot of percent difference in MSE between HNNs and their corresponding PBMs in the training phase as a function of the number of predictor variables used in the HNN. (B) Histogram of percent difference in MSE between HNNs and their corresponding PBMs in the training phase (local-converged HNNs excluded). All negative percent difference were set to 0.1% for visualization purposes. The blue shaded portion represent those HNNs with only two predictor variables. (For interpretation of the references to colour in this figure legend, the reader is referred to the Web version of this article.)

Table 2
HNN and PBM results for the best performing HNNs that use only two predictor variables.

Predicted soils	MSE, HNN	MSE, PBM	$f(z)$	$\Gamma_{ini} \cdot \hat{k}$
Model 7a with $f(t,T)$ trained to SCT1,2,3,5, Panola				
SCT1,2,3,5, Panola (training)	0.0033	0.0033	–	–
Davis	0.18	0.001	1.2	0.58
Jughandle	0.023	0.015	1.1	0.88
Model 7b with $f(t,T)$ trained to SCT1,2,3,5, Davis				
SCT1,2,3,5, Davis (training)	0.0031	0.003	–	–
Panola	0.17	0.0038	0.62	1.2
Jughandle	0.029	0.015	0.68	0.88
Model 9a with $f(t,E)$ trained to SCT1,2,3,5, Panola				
SCT1,2,3,5, Panola (training)	0.0033	0.0033	–	–
Davis	0.18	0.001	1.2	0.58
Jughandle	0.021	0.015	0.88	0.88
Model 11a with $f(t,A)$ trained to SCT1,2,3,5, Panola				
SCT1,2,3,5, Panola (training)	0.0033	0.0033	–	–
Davis	0.18	0.001	1.2	0.58
Jughandle	0.017	0.015	0.98	0.88
Model 11c with $f(t,A)$ trained to SCT1,2,3,5				
SCT1,2,3,5 (training)	0.0031	0.0031	–	–
Panola	0.14	0.0038	0.82	1.2
Davis	0.064	0.001	0.82	0.58
Jughandle	0.019	0.015	0.81	0.88
Model 14a with $f(T,Q)$ trained to SCT1,2,3,5, Panola				
SCT1,2,3,5, Panola (training)	0.0033	0.0033	–	–
Davis	0.27	0.001	−0.47	0.58
Jughandle	0.072	0.015	0.14	0.88
Model 14b with $f(T,Q)$ trained to SCT1,2,3,5, Davis				
SCT1,2,3,5, Davis (training)	0.003	0.003	–	–
Panola	0.085	0.0038	1.7	1.2
Jughandle	0.051	0.015	0.48	0.88

set.

As for f(t,A), it was successfully trained with "a" and "c" series training sets but not with the "b" series training set. A comparison of MSE values of HNN 11b and those HNNs using a subset of predictor variables used by 11b indicated that HNN model 1b f(t) was 82% better than HNN 11b in terms of MSE values. Therefore, we inferred that HNN 11b was likely converged locally, and it was excluded from the list of best performing HNNs.

4.3. Comparison of HNN models to validation data

Trained HNNs were also applied to predict the reaction front for those soil profiles not included in the training set. Reaction fronts predicted by the HNN and by the corresponding PBM were plotted for all the seven best performing HNNs in Figs. 7–9. The depth profiles of

normalized measured Na concentrations are also shown for comparison. However, given that HNNs were trained on some of the profiles, not all profiles are plotted for all HNN predictions. For example, for HNNs trained with the "a" series training set, only soil profiles for Davis Run and Jughandle were tested because Panola was used in training (Fig. 7). Likewise, for HNNs trained with the "b" series training set, soil profiles of Panola and Jughandle were tested (Fig. 8). For HNNs trained with the "c" series training set (trained only SCT profiles), we tested the trained model with soil profiles of Davis Run, Panola, and Jughandle (Fig. 9).

In general, trained HNNs can mostly predict the slope of the reaction front very well as compared to the corresponding PBM. We did not expect the models to predict the depth of the soil profile as well as the PBM. From Eqn. (5), we know that the initial guess for $\Gamma_{ini}\cdot\hat{k}$ in the PBM depends on the slope of the reaction front. The HNN, which ultimately predicts $\Gamma_{ini}\cdot\hat{k}$ in a data-driven way, in essence, is able to find the slope of the soil profile which yields a quantification for the ratio of rate of dissolution of the albitic feldspar and the rate of transport. However, Eqn. (6) shows that the initial guess for $C_{x=0}$ depends on both $\Gamma_{ini}\cdot\hat{k}$ and the depth of the soil profile. So, since the HNN keeps the same $C_{x=0}$ value as the PBM while seeking potentially different values of $\Gamma_{ini}\cdot\hat{k}$, HNN's prediction for the depth of the soil profile is relatively inaccurate.

5. Conclusions

In this study we explored whether we could use hybrid neural networks (HNN), i.e., a neural network guided by a physics-based model (PBM), to predict concentration-depth data for reaction fronts in soils. We tested the idea that an HNN might teach us which variables that control soil formation are the most important in controlling reaction fronts. We specifically tested soil residence time (t), site climate characteristics [mean annual temperature (T), precipitation (P)], site erosion rate (E), quartz content (Q) of the parent material, and/or albite content (A) of the feldspar. For each of the 63 combinations of these environmental predictor variables, we trained and tested an HNN for comparison to a PBM for three different sets of soil training and test datasets. To seek the best performing HNN in terms of mimicking the prediction results from the corresponding PBM, we evaluated the percent difference in MSE (1) between each of the HNNs and any HNNs using the same subset of predictor variables in the training phase, and (2) between HNNs and their corresponding PBMs in the training phase. Among those best performing HNNs, soil residence time (t) was most frequently included as a predictor variable in the HNNs.

The HNN thus taught us that soil residence/exposure time is the most useful predictor variable in terms of predicting the slope of a reaction
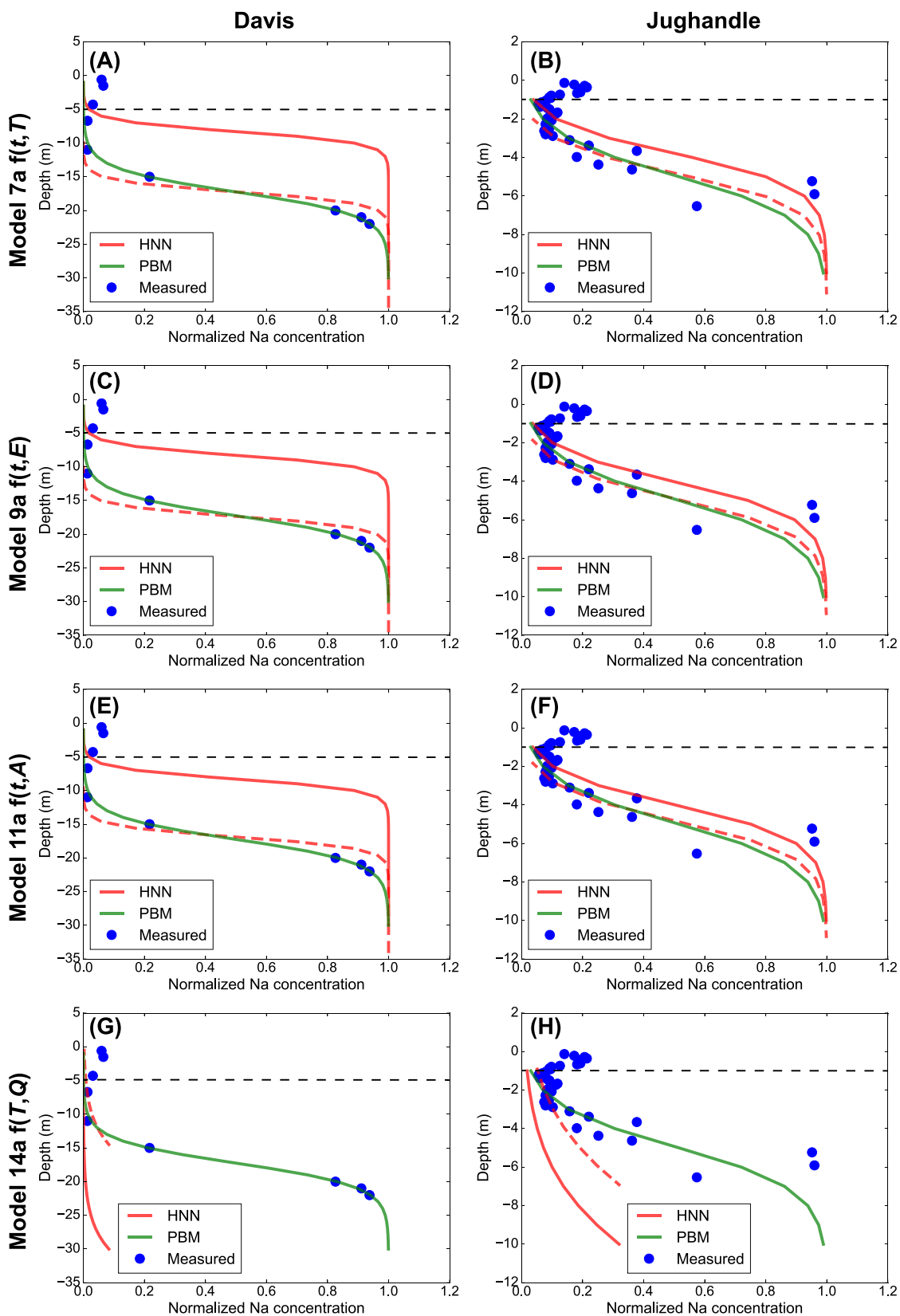
Fig. 7. Normalized Na concentration (measured, blue symbols) plotted versus depth with results from the PBM fitted to the individual data points (green line) and the HNN results for each soil profile (red line). Panels (A), (C), (E), and (G) are for the Davis soil profile while panels (B), (D), (F), and (H) are for the Jughandle soil profile. (A) and (B), (C) and (D), (E) and (F), and (G) and (H) show results from HNN models 7a, 9a, 11a, and 14a, respectively. Note: red dashed curves represent HNN prediction results with a vertical offset to facilitate the comparison of the slope of PBM and HNN results. The black dashed line denotes the boundary above which soil samples might include exogenous disturbance (e.g., eolian input and bioturbation). (For interpretation of the references to colour in this figure legend, the reader is referred to the Web version of this article.)
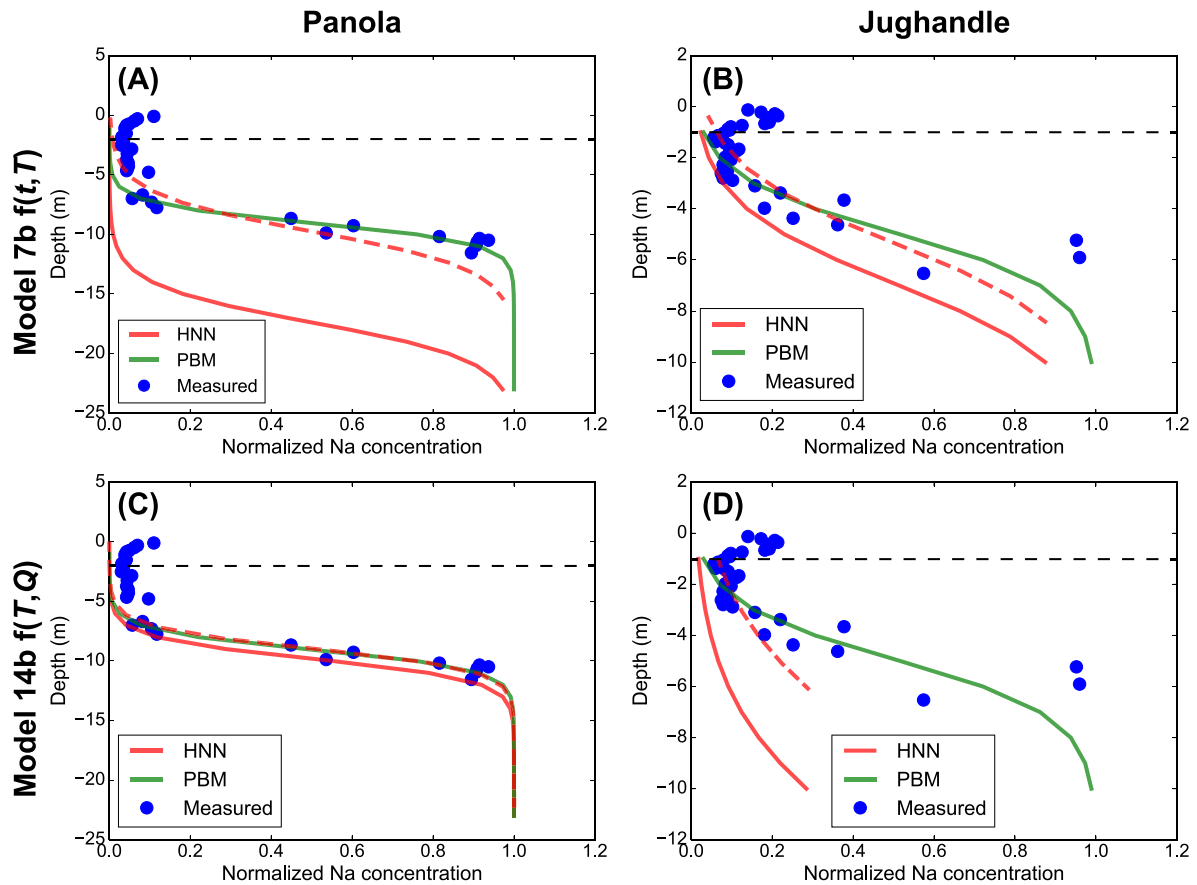
Fig. 8. Normalized Na concentration (measured, blue symbols) plotted versus depth with results from the PBM fitted to the individual data points (green line) and the HNN results for each soil profile (red line). Panels (A) and (C) are for the Panola soil profile while panels (B) and (D) are for the Jughandle soil profile. (A) and (B), and (C) and (D) show results from HNN models 7b and 14b, respectively. Note: red dashed curves represent HNN prediction results with a vertical offset to facilitate the comparison of the slope of PBM and HNN results. The black dashed line denotes the boundary above which soil samples might include exogenous disturbance (e. g., eolian input and bioturbation). (For interpretation of the references to colour in this figure legend, the reader is referred to the Web version of this article.)
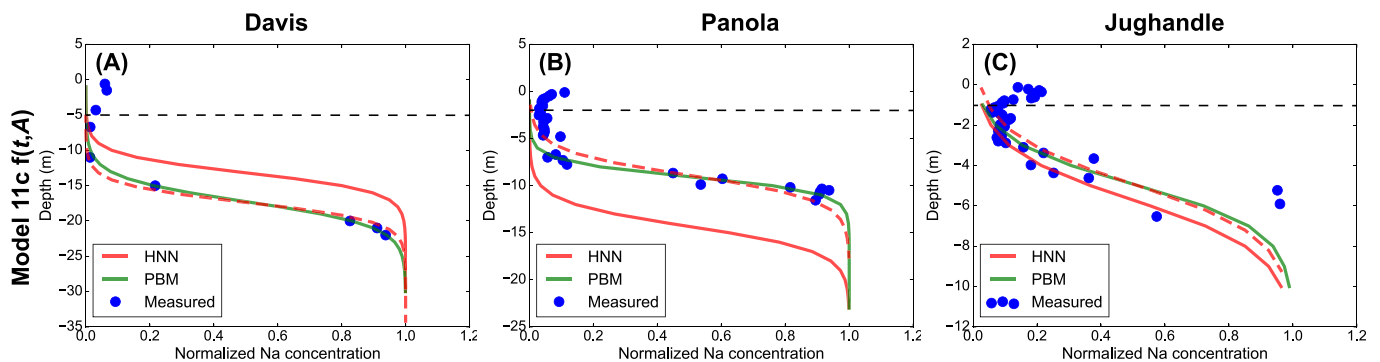

Fig. 9. Normalized Na concentration (measured, blue dot) plotted versus depth with results from the PBM fitted to the individual data points (green line) and the HNN 11c results (red line) for soil profiles of (A) Davis, (B) Panola, and (C) Jughandle. Note: red dashed curves represent HNN prediction results with a vertical offset to facilitate the comparison of the slope of PBM and HNN results. The black dashed line denotes the boundary above which soil samples might include exogenous disturbance (e.g., eolian input and bioturbation). (For interpretation of the references to colour in this figure legend, the reader is referred to the Web version of this article.)

front, an observable that is related in some soils to the advective Damköhler number of the weathering system (e.g., Brantley and Lebedeva, 2021; von Blanckenburg et al., 2021). Surprisingly, precipitation was the least useful predictor variable. We also explored how adding additional predictor variables might contribute to the improvement of prediction accuracy of HNNs. The preliminary results showed that at least two predictor variables were needed for an HNN to achieve an MSE within 1% different of the corresponding PBM. Trained best performing

HNNs were also used to predict the reaction front for soil profiles not included in the corresponding training dataset. Prediction results showed that HNNs can generally mimic the PBM-simulated reaction front with respect to the front's slope but not with respect to the depth of the front, a result that is at least partly related to the limitation of the original PBM equation.

This is the first time an NN was incorporated into a PBM to develop an HNN to simulate the depth profile of soil geochemistry. Although the

proposed HNN consisted of only two layers and a small number of predictor variables, the preliminary results of our work indeed pointed out a promising direction for the application of NN in the even more complex PBM (e.g., high resolution reactive transport models): replacing the sub-model of a PBM with a machine learning model to either simplify the complicated parametrization that might be in high demand of domain knowledge or to improve the computational efficiency as the machine learning models usually run a lot faster than the corresponding physics sub-model (e.g., Prasianakis et al., 2020; Reichstein et al., 2019). This requires that NN/HNN models be generalized to more soil profiles (Mojid et al., 2019) and be improved to incorporate automation of NN/HNN training (Prasianakis et al., 2020).

Computer code availability

All hybrid neural network models in this study are implemented using the TensorFlow 1.13.1 with the Python 3.5. Source codes of model development and application as well as the associated input data can be downloaded from the corresponding GitHub repository via this link: http://doi.org/10.5281/zenodo.6974714.

CRediT authorship contribution statement

Tao Wen: Supervision, Conceptualization, Investigation, Writing – original draft, Writing – review & editing. Chacha Chen: Conceptualization, Investigation, Writing – original draft, Writing – review & editing. Guanjie Zheng: Conceptualization, Investigation, Writing - review & editing. Joel Bandstra: Supervision, Conceptualization, Investigation, Writing - review & editing. Susan L. Brantley: Funding acquisition, Supervision, Conceptualization, Investigation, Writing – review & editing.

Declaration of competing interest

The authors declare that they have no known competing financial interests or personal relationships that could have appeared to influence the work reported in this paper.

Appendix A. Supplementary data

Supplementary data to this article can be found online at https://doi.org/10.1016/j.cageo.2022.105200.

References

Bandstra, J.Z., Tratnyek, P.G., 2004. Applicability of single-site rate equations for reactions on inhomogeneous surfaces. Ind. Eng. Chem. Res. 43, 1615–1622. https://doi.org/10.1021/ie034250a.

Bergen, K.J., Johnson, P.A., Hoop, M.V., Beroza, G.C., 2019. Machine learning for data-driven discovery in solid Earth geoscience. Science 363, 1299. https://doi.org/10.1126/science.aau0323.

Beven, K., Freer, J., 2001. Equifinality, data assimilation, and uncertainty estimation in mechanistic modelling of complex environmental systems using the GLUE methodology. J. Hydrol. 249, 11–29.

Bierman, P., Gillespie, A., Caffee, M., Elmore, D., 1995. Estimating erosion rates and exposure ages with 36Cl produced by neutron activation. Geochem. Cosmochim. Acta 59, 3779–3798. https://doi.org/10.1016/0016-7037(95)00267-4.

Blum, A., Stillings, L.L., 1995. Feldspar dissolution kinetics. In: White, A.F., Brantley, S.L. (Eds.), Chemical Weathering Rates of Silicate Mineral: an Overview. Mineralogical Society of America, pp. 291–351.

Brantley, S.L., Bandstra, J., Moore, J., White, A.F., 2008. Modelling chemical depletion profiles in regolith. Geoderma 145, 494–504. https://doi.org/10.1016/j.geoderma.2008.02.010.

Brantley, S.L., Lebedeva, M., 2011. Learning to read the chemistry of regolith to understand the Critical Zone. Annu. Rev. Earth Planet Sci. 39, 387–416.

Brantley, S.L., Lebedeva, M.I., 2021. Relating land surface, water table, and weathering fronts with a conceptual valve model for headwater catchments. Hydrol. Process. 35 https://doi.org/10.1002/hyp.14010.

Brantley, S.L., Lebedeva, M.I., Balashov, V.N., Singha, K., Sullivan, P.L., Stinchcomb, G., 2017. Toward a conceptual model relating chemical reaction fronts to water flow paths in hills. Geomorphology 277, 100–117. https://doi.org/10.1016/j.geomorph.2016.09.027.

Brantley, S.L., White, A.F., 2009. Approaches to modeling weathered regolith. Rev. Mineral. Geochem. 435–484.

Brimhall, G.H., Dietrich, W.E., 1987. Constitutive mass balance relations between chemical composition, volume, density, porosity, and strain in metasomatic hydrochemical systems: results on weathering and pedogenesis. Geochem. Cosmochim. Acta 51, 567–587.

Brouwer, W.J., Kubicki, J.D., Sofo, J.O., Giles, C.L., 2014. An Investigation of Machine Learning Methods Applied to Structure Prediction in Condensed Matter.

Cybenko, G., 1989. Approximation by superpositions of a sigmoidal function. Math. Control, Signals, Syst. MCSS 2, 303–314.

Dokuchaev, V.V., 1883. Russian Chernozem Selected Works of V.V.

Eckert, A.J., Shahi, H., Datwyler, S.L., Neale, D.B., 2012. Spatially variable natural selection and the divergence between parapatric subspecies of lodgepole pine (pinus contorta, pinaceae. Am. J. Bot. 99, 1323–1334.

Godderis, Y., Schott, J., Brantley, S.L., 2019. Reactive transport models of weathering. Elements 1, 103–106. https://doi.org/10.2138/gselements.15.2.103.

Goodfellow, I., Bengio, Y., Courville, A., 2016. Deep Learning. MIT Press.

Hornik, K., Stinchcombe, M., White, H., 1989. Multilayer feedforward networks are universal approximators. Neural Network. 2, 359–366. https://doi.org/10.1016/0893-6080(89)90020-8.

Hornik, K., 1991. Approximation capabilities of multilayer feedforward networks. Neural Network. 4, 251–257.

Jenny, H., 1941. The Factors of Soil Formation. McGraw Hill, New York.

Karpatne, A., Atluri, G., Faghmous, J.H., Steinbach, M., Banerjee, A., Ganguly, A., Shekhar, S., Samatova, N., Kumar, V., 2017. Theory-guided data science: a new paradigm for scientific discovery from data. IEEE Trans. Knowl. Data Eng. 29, 2318–2331. https://doi.org/10.1109/TKDE.2017.2720168.

Kingma, D.P., Ba, J., 2014. Adam: A Method for Stochastic Optimization.

Laloy, E., Jacques, D., 2019. Emulation of CPU-demanding reactive transport models: a comparison of Gaussian processes, polynomial chaos expansion, and deep neural networks. Comput. Geosci. 23, 1193–1215.

Lebedeva, M.I., Fletcher, R.C., Balashov, V.N., Brantley, S.L., 2007. A reactive diffusion model describing transformation of bedrock to saprolite. Chem. Geol. 244, 624–645. https://doi.org/10.1016/j.chemgeo.2007.07.008.

Lebedeva, M.I., Fletcher, R.C., Brantley, S.L., 2010. A mathematical model for steady-state regolith production at constant erosion rate. Earth Surf. Process. Landforms. https://doi.org/10.1002/esp.1954 n/a-n/a.

LeCun, Y., Bengio, Y., Hinton, G., 2015. Nature 521, 436–444.

Li, L., Maher, K., Navarre-Sitchler, A., Druhan, J., Meile, C., Lawrence, C., Moore, J., Perdrial, J., Sullivan, P., Thompson, A., Jin, L., Bolton, E.W., Brantley, S.L., Dietrich, W.E., Mayer, K.U., Steefel, C.I., Valocchi, A., Zachara, J., Kocar, B., Mcintosh, J., Tutolo, B.M., Kumar, M., Sonnenthal, E., Bao, C., Beisman, J., 2017. Expanding the role of reactive transport models in critical zone processes. Earth Sci. Rev. 165, 280–301. https://doi.org/10.1016/j.earscirev.2016.09.001.

Lichtner, P.C., 1988. The quasi-stationary state approximation to coupled mass transport and fluid-rock interaction in a porous medium. Geochem. Cosmochim. Acta 52, 143–165.

Lichtner, P.C., Steefel, C.I., Oelkers, E.H., 1996. Reactive transport in porous media. Rev. Mineral. 34, 438.

Livingstone, D.J., Manallack, D.T., Tetko, I.V., 1997. Data modelling with neural networks: advantages and limitations. J. Comput. Aided Mol. Des. 8.

Maher, K., Navarre-Sitchler, A., 2019. Reactive transport processes that drive chemical weathering: from making space for water to dismantling continents. Rev. Mineral. Geochem. 349–380.

Maher, K., Steefel, C.I., White, A.F., Stonestrom, D.A., 2009. The role of reaction affinity and secondary minerals in regulating chemical weathering rates at the Santa Cruz Soil Chronosequence, California. Geochem. Cosmochim. Acta 73, 2804–2831. https://doi.org/10.1016/j.gca.2009.01.030.

Masiello, C.A., Chadwick, O.A., Southon, J., Torn, M.S., Harden, J.W., 2004. Weathering controls on mechanisms of carbon storage in grassland soils. Global Biogeochem. Cycles 18, 9.

Merrill, G.P., 1906. A Treatise on Rocks, Rock Weathering and Soils. MacMillian Inc, New York.

Merritts, D., Bull, W.B., 1989. Interpreting quaternary uplift rates at the mendocino triple junction, northern California, from uplifted marine terraces. Geology 17, 1020–1024.

Merritts, D.J., Chadwick, O.A., Hendricks, D.M., 1991. Rates and processes of soil evolution on uplifted marine terraces, northern California. Geoderma 51, 241–275.

Mojid, M.A., Hossain, A.B.M.Z., Ashraf, M.A., 2019. Artificial neural network model to predict transport parameters of reactive solutes from basic soil properties. Environ. Pollut. 255 https://doi.org/10.1016/j.envpol.2019.113355.

Moore, J., Lichtner, P.C., White, A.F., Brantley, S.L., 2012. Using a reactive transport model to elucidate differences between laboratory and field dissolution rates in regolith. Geochem. Cosmochim. Acta 93, 235–261.

Northup, R.R., Dahlgren, R.A., Yu, Z., 1995. Intraspecific variation of conifer phenolic concentration on a marine terrace soil acidity gradient; a new interpretation. Plant Soil 171, 255–262. https://doi.org/10.1007/BF00010279.

Pavich, M.J., 1986. Processes and rates of saprolite production and erosion on a foliated granitic rock of the Virginia piedmont. In: Colman, S.M., Dethier, D.P. (Eds.), Rates of Chemical Weathering of Rocks and Minerals. Academic Press, Orlando, FL, p. 603.

Pavich, M.J., Brown, L., Valette-Silver, J.N., Klein, J., Middleton, R., 1985. 10Be analysis of a Quaternary weathering profile in the Virginia Piedmont. Geology 13, 39–41. https://doi.org/10.1130/0091-7613(1985)13<39:BAOAQW>2.0.CO;2.

Prasianakis, N.I., Haller, R., Mahrous, M., Poonoosamy, J., Pfingsten, W., Churakov, S.V., 2020. Neural network based process coupling and parameter upscaling in reactive transport simulations. Geochem. Cosmochim. Acta 291, 126–143. https://doi.org/10.1016/j.gca.2020.07.019.

Press, W.H., Teukolsky, S.A., Vetterling, W.T., Flannery, B.P., 2007. Numerical Recipes: the Art of Scientific Computing. Cambridge University Press.

Reichstein, M., Camps-Valls, G., Stevens, B., Jung, M., Denzler, J., Carvalhais, N., Prabhat, 2019. Deep learning and process understanding for data-driven Earth system science. Nature 566, 195–204. https://doi.org/10.1038/s41586-019-0912-1.

Riebe, C.S., Hahm, W.J., Brantley, S.L., 2016. Controls on deep critical zone architecture: a historical review and four testable hypotheses. Earth Surf. Process. Landforms 42, 128–156. https://doi.org/10.1002/esp.4052.

Savenije, H.H.G., 2001. Equifinality, a blessing in disguise? Hydrol. Process. 15, 2835–2838.

Schmidt, M., Lipson, H., 2009. Distilling free-form natural laws form experimental data. Science 324, 81–85.

Schulz, K., Beven, K., H, B., 1999. Equifinality and the problem of robust calibration in nitrogen budget simulations. Soil Sci. Soc. Am. J. 63, 1934–1941.

Shen, C., Laloy, E., Elshorbagy, A., Albert, A., Bales, J., Chang, F.-J., Ganguly, S., Hsu, K.-L., Kifer, D., Fang, Z., Fang, K., Li, D., Li, X., Tsai, W.-P., 2018. HESS Opinions: incubating deep-learning-powered hydrologic science advances as a community. Hydrol. Earth Syst. Sci. 22, 5639–5656. https://doi.org/10.5194/hess-22-5639-2018.

Shen, C.P., 2018. A transdisciplinary review of deep learning research and its relevance for water resources scientists. Water Resour. Res. 54, 8558–8593.

Tang, J., Zhuang, Q., 2008. Equifinality in parameterization of process-based biogeochemistry models: a significant uncertainty source to the estimation of regional carbon dynamics. J. Geophys. Res.: Biogeosciences 113.

Uroz, S., Tech, J.J., Sawaya, N.A., Frey-Klett, P., Leveau, J.H.J., 2014. Structure and function of bacterial communities in ageing soils: insights from the Mendocino ecological staircase. Soil Biol. Biochem. 69, 265–274.

von Blanckenburg, F., Schuessler, J.A., Bouchez, J., Frings, P.J., Uhlig, D., Oelze, M., Frick, D.A., Hewawasam, T., Dixon, J., Norton, K., 2021. Rock weathering and nutrient cycling along an erodosequence. Am. J. Sci. 321, 1111–1163. https://doi.org/10.2475/08.2021.01.

Washton, N.M., Brantley, S.L., Mueller, K.T., 2008. Probing the molecular-level control of aluminosilicate dissolution: a sensitive solid-state NMR proxy for reactive surface area. Geochem. Cosmochim. Acta 72, 5949–5961. https://doi.org/10.1016/j.gca.2008.09.018.

White, A.F., Brantley, S.L., 2003. The effect of time on the weathering of silicate minerals: why do weathering rates differ in the laboratory and field? Chem. Geol. 202, 479–506. https://doi.org/10.1016/j.chemgeo.2003.03.001.

White, A.F., Bullen, T.D., Schulz, M.S., Blum, A.E., Huntington, T.G., Peters, N.E., 2001. Differential rates of feldspar weathering in granitic regoliths. Geochem. Cosmochim. Acta 65, 847–869. https://doi.org/10.1016/S0016-7037(00)00577-9.

White, A.F., Schulz, M.S., Stonestrom, D.A., Vivit, D.V., Fitzpatrick, J., Bullen, T.D., Maher, K., Blum, A.E., 2009. Chemical weathering of a marine terrace chronosequence, Santa Cruz, California. Part II: solute profiles, gradients and the comparisons of contemporary and long-term weathering rates. Geochem. Cosmochim. Acta 73, 2769–2803. https://doi.org/10.1016/j.gca.2009.01.029.

White, A.F., Schulz, M.S., Vivit, D.V., Blum, A.E., Stonestrom, D.A., Anderson, S.P., 2008. Chemical weathering of a marine terrace chronosequence, Santa Cruz, California I: interpreting rates and controls based on soil concentration–depth profiles. Geochem. Cosmochim. Acta 72, 36–68. https://doi.org/10.1016/j.gca.2007.08.029.